The surface roughness effect on electrochemical properties of La0.5Sr0.5Fe0.7Ga0.3O3-δ perovskite for oxygen transport membranes

L. Guironnet, P.-M. Geffroy, N. Tessier-Doyen, A. Boulle, N. Richet, T. Chartier

The surface roughness effect on electrochemical properties of $La_{0.5}Sr_{0.5}Fe_{0.7}Ga_{0.3}O_{3-\delta}$ perovskite for oxygen transport membranes

L. Guironnet[1,3], P.-M. Geffroy[1,*], N. Tessier-Doyen[1], A. Boulle[1], N. Richet[2], T. Chartier[1]

[1] IRCER, CNRS, ENSCI, Université de Limoges. CEC. 12 Rue Atlantis 87068 Limoges. France
[2]Air Liquide CRCD, 1 chemin de la Porte des Loges, BP126, 78354 Jouy en Josas, France
[3]ADEME, 20 rue du Grésillé – BP90406, 49004 Angers Cedex 01, France

***Corresponding Author:**
Pierre-Marie Geffroy
Affiliation: IRCER, CNRS, Université de Limoges,
Address: 12 rue Atlantis 87068 Limoges, France,
Phone: 05 87 50 23 53,
Fax: 05 87 50 23 04,
E-mail : pierre-marie.geffroy@unilim.fr

Abstract

The effect of the membrane surface on the oxygen permeation performances is not studied to sufficient detail in the literature. However, this paper shows that the roughness, and the surface physico-chemistry can have a large effect on the oxygen semi-performances of the membrane, in particular on the kinetics of oxygen exchanges at the surface of the mixed electronic and ionic conductors. For instance, the kinetic coefficient of oxygen surface exchanges can increase by more than one order of magnitude in relation with the surface roughness for $La_{0.5}Sr_{0.5}Fe_{0.7}Ga_{0.3}O_{3-\delta}$ perovskite-type membrane. Then, the best oxygen fluxes obtained in this work, i.e. $3.9\ 10^{-3}$ $mol.m^{-2}.s^{-1}$, are close to the best performances reported in the literature for a dense 1 mm in thick membrane. Finally, some assumptions are discussed and argued in detail to explain the effect of the surface of the $La_{0.5}Sr_{0.5}Fe_{0.7}Ga_{0.3}O_{3-\delta}$ perovskite membrane on their oxygen semi-permeation performances.

Keywords: surface roughness, oxygen surface exchanges, oxygen semi-permeation, mixed electronic ionic conductors

1. Introduction

The oxygen transport membranes (OTM) are dense ceramic membranes usually manufactured using mixed ionic and electronic conductor materials. The electromotive force of the oxygen transport through the membrane is linked to the difference of oxygen partial pressures imposed between the two atmospheres on either side of the

membrane. However, the oxygen flux produced by the ceramic membranes is not enough high for an industrial development [1,2]. Numerous studies reported in the literature aim to better understand the main mechanisms of oxygen transport through the membrane, in order to improve their performances of oxygen semi-permeation. The majority of these studies reported that the oxygen flux though the membrane is governed by the kinetic of oxygen surface exchanges at the oxygen lean surface of the membrane. In this respect, a coating of ultra-divided particles or a porous coating on the membrane surface significantly improves oxygen flux through the membrane [3-5].

The effect of the roughness of the membrane surface on the oxygen semi-permeation performances is rarely studied. Tereaoka [6] or Gurauskis et al. [7-10] show that the oxygen semi-permeation flux through $La_{0.1}Sr_{0.9}Fe_{0.1}Co_{0.9}O_{3-\delta}$ and $La_{0.2}Sr_{0.8}Fe_{0.8}Ta_{0.2}O_{3-\delta}$ perovskite membranes increases with the surface roughness of the membrane. Indeed, the surface quality of the membrane can lead to a variation of the oxygen semi-permeation flux, if the oxygen flux through the membrane is governed by oxygen surface exchanges kinetics [6, 10]. Then, Wang [11] and Shaomin et al. [12] reported that the surface treatment by acid etching of K_2NiF_4-type oxide membranes leads to improve the oxygen permeation performances and the oxygen surface exchange kinetics.

Besides, R.J. Carter et al. show than the apparent coefficient of oxygen surface exchange (k*), determined by the isotopic exchanges method, usually increases with the roughness of sample surface [13]. Then, the determination of k* obtained by the isotopic exchanges method suggests to control the surface finish of the sample.

This work aims to evaluate the influence of the surface roughness on the oxygen flux through $La_{0.5}Sr_{0.5}Fe_{0.7}Ga_{0.3}O_{3-\delta}$ perovskite-type membrane ($LSFG_{5573}$) and, in particular on the kinetic coefficient of oxygen surface exchange of the membrane materials. The $LSFG_{5573}$ material is of great interest as membrane material, with the advantages of good chemical stability [14] in long duration tests, mechanical properties and high oxygen diffusion coefficient. Nevertheless, the main drawback of this material is a very low kinetic coefficient of oxygen surface exchange [8].

2. Experimental part

2.1 Materials

The $La_{0.5}Sr_{0.5}Fe_{0.7}Ga_{0.3}O_{3-\delta}$ ($LSFG_{5573}$) perovskite-type powder is synthesized using a solid state reaction synthesis route. Pure oxides (La_2O_3 (99.99 %, Alfa Aesar), Fe_2O_3 (98 %, Alfa Aesar), Ga_2O_3 (99.999 %, Alfa

Aesar)) are dehydrated at 100 °C. Then, dry oxides and carbonate ($SrCO_3$ (99.9 %, Sigma-Aldrich)) precursors are weighed in the stoichiometric amount, mixed and attrition-milled at 600 rpm in ethanol media. The attrition milling is performed using 0.8 mm diameter zirconia balls. After 3 h, the mixture is separated from the zirconia balls with a 200 µm sieve, dried and calcined 5h at 1100°C. After calcination step, the perovskite phase is obtained, and the powder is once again attrition-milled in ethanol media during 3 hours to obtain a monomodal grain size distribution centered on 1 µm (laser granulometer - Horiba LA950). The chemical composition of the synthesized powder is determined by inductively coupled plasma atomic emission spectrometer (ICP-AES).

2.2 Elaboration of membrane samples

The membrane samples are elaborated by tape casting, as reported in previous works [15, 16]. A $LSFG_{5573}$ suspension is prepared from the synthesized powder, an organic solvent, a dispersant (phosphate ester), a binder (polymethacrylate) and a plasticizer (dibutyl phalate). The synthesized powder is first deagglomerated/dispersed for 1h in the organic solvent with the dispersant using ball-milling at 210 r.p.m. Then, the binder and the plasticizer are added and mixed to the slurry using ball-milling at 120 r.p.m for 12 h. The thickness of green tapes obtained by tape casting is 150 µm. The green tape is stamped into 30 mm diameter disks. Then, the disks are stacked and thermo-laminated under 50 MPa at 70 °C (in order to obtain 1 mm thick sintered disks). The green membranes are debinded and sintered at 1330 °C for 2h at a rate of 1 °C/min to obtain a relative density larger than 95% (Archimedes method).

2.3 Surface finishing of membrane samples

The surfaces of $LSFG_{5573}$ membranes are polished with 3 various abrasive papers (SiC) in order to obtain different surface roughness. The “P120” membrane is roughly polished with a P120 grade-type abrasive paper, the “P600” membrane is polished with a softer abrasive paper and the “MP” membrane is mirror-polished. Each membranes were cleaned in an ethanol ultrasonic bath for ten minutes to eliminate the residual particles of silicon carbide. The roughness of the surfaces is measured by white light interferometry microscope (Fogale nanotech). The final thickness of membrane sample is adjusted during the polishing to be close to 1mm (+/- 0.05 mm).

Structural characterizations of the membrane surface are carried out using grazing incidence X-ray diffraction (Bruker D8 Discover diffractometer, equipped with a copper source). A parabolic mirror coupled to a 2 reflections asymmetrical Germanium monochromator allows to select the Cu $K\alpha_1$ wavelength and produces a

parallel bean. The sample is positioned on a 5-axis goniometer. The detection is carried out using a LynxEye-type linear detector, covering an angular range of 2° with a resolution of 0.01°.

2.4 The oxygen semi-permeation performances of membrane samples

2.4.1 *The setup for oxygen semi-permeation measurements*

Electrochemical performances, i.e. oxygen semi-permeation flux, and oxygen activities at the membrane surfaces are measured using a specific setup given Figure 1 and described in previous works [17, 18]. The membrane is sealed between two alumina tubes by gold rings [19]. In the first chamber, recombined air is injected (100 mL/min, oxygen-rich atmosphere), in the second chamber, argon is injected (200 mL/min, oxygen-lean atmosphere). The oxygen partial pressure gradient through the membrane or between the chamber 1 and 2, is the driving force for oxygen diffusion through the membrane. The chamber 3 prevents the eventual leakages between the chamber 1 and 2. The oxygen semi-permeation measurements are performed from 970 °C to 600°C with an interval of 10 °C between each measure.

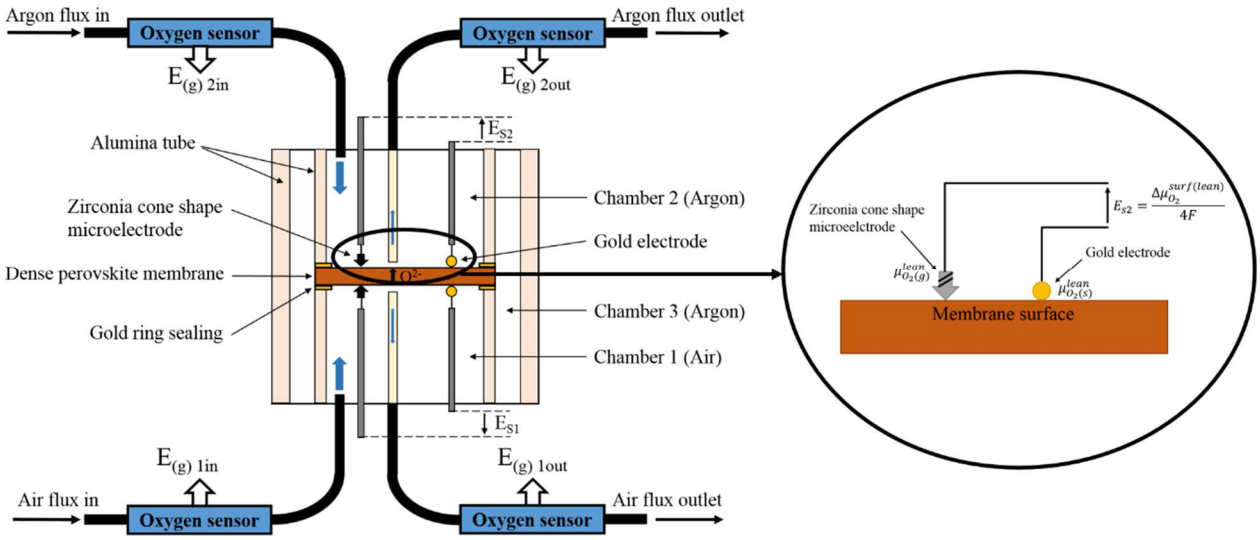

Figure 1. Oxygen semi-permeation setup and its microelectrodes system

2.4.2 Oxygen semi-permeation measurements

The oxygen flux through the membrane is evaluated using the following equation:

$$J_{O_2} = \frac{D_{Ar}}{S\ V_{m(Ar)}}\ (P_{2out} - P_{2e}) \quad \textbf{(Eq. 1)}$$

where J_{O_2} is the oxygen flux through the membrane in mol.m^{-2}.s^{-1}, D_{Ar} the argon flow in l.s^{-1}, $V_{m(Ar)}$ the molar volume of argon in l.mol^{-1} and S the effective membrane surface in m^2. P_{2out} and P_{2e} are the oxygen partial

pressure in the outlet argon flux and the oxygen partial pressure in the argon flux (in atm), respectively. They are evaluated from the electromotive force $E_{(g)\,2out}$, thanks to YSZ-oxygen sensors, following the Nernst law:

$$E_{(g)2out} = \frac{RT}{4F} \ln \frac{P_{2out}}{P_{O_2}} \quad \textbf{(Eq. 2)}$$

where R is the universal gas constant, F the Faraday constant, T the temperature and P_{O2} is the oxygen partial pressure in the air (= 0.21 atm.).

The particularity of this apparatus is the possibility to determine the oxygen activity at the both surfaces of the membrane. The microelectrodes system, composed of a gold electrode and a zirconia tip, in contact with the surface measures two electromotive forces E_{s1} and E_{s2}, respectively the variation of oxygen activities between the inlet gas and the oxygen-rich or lean surfaces of the membrane [20]. The gradients of di-oxygen activity on each surface of the membrane are evaluated from the Nernst law:

$$E_{S1} = \frac{RT}{4F} \ln \frac{a_1}{a\prime_1} = \frac{\Delta\mu^{rich}_{O_{2(s)}}}{4F} \quad \textbf{(Eq. 3)}$$

$$E_{S2} = \frac{RT}{4F} \ln \frac{a\prime_2}{a_2} = \frac{\Delta\mu^{lean}_{O_{2(s)}}}{4F} \quad \textbf{(Eq. 4)}$$

where $\Delta\mu^{lean}_{O_{2(s)}} = \mu^{lean}_{O_{2(s)}} - \mu^{lean}_{O_{2(g)}}$ and $\Delta\mu^{rich}_{O_{2(s)}} = \mu^{rich}_{O_{2(g)}} - \mu^{rich}_{O_{2(s)}}$

$\mu^{rich}_{O_{2(g)}}$ and $\mu^{lean}_{O_{2(g)}}$ are the oxygen chemical potentials in air and argon. $\mu^{rich}_{O_{2(s)}}$ and $\mu^{lean}_{O_{2(s)}}$ are the oxygen chemical potentials on oxygen-rich and oxygen-lean surfaces, respectively.

The difference between the oxygen chemical potential $\mu^{lean}_{O_{2(s)}}$ and $\mu^{rich}_{O_{2(s)}}$ corresponds to the gradient of oxygen chemical activity in the bulk of the membrane, noted $\Delta\mu^{Bulk}_{O_2}$.

2.4.3 Determination of oxygen surface exchange coefficients

k_i and k_{des} are respectively the kinetic coefficients of oxygen surface exchange at oxygen-rich surface and at oxygen-lean surface of the membrane, expressed in $cm.s^{-1}$. They are described from the formalism recently reported by Bazan et al. [21] or Adler et al. [22] and calculated from the oxygen semi-permeation flux and the gradient of oxygen chemical potential at the membrane surface, as following:

$$k_i = 2J_{O_2} \Big/ \left(C_0^{rich} \left(\exp\left(\frac{(1-n)\Delta\mu^{rich}_{O_{2(s)}}}{2RT} \right) - \exp\left(\frac{-n\Delta\mu^{rich}_{O_{2(s)}}}{2RT} \right) \right) \right) \quad \textbf{(Eq. 5)}$$

$$k_{des} = 2J_{O_2} \Big/ \left(C_0^{lean} \left(\exp\left(\frac{(1-n)\Delta\mu_{O_{2(s)}}^{lean}}{RT} \right) - \exp\left(\frac{-n\Delta\mu_{O_{2(s)}}^{lean}}{RT} \right) \right) \right) \textbf{(Eq. 6)}$$

where n is a coefficient typically equal to 0.5 for MIEC materials and C_0^{rich} and C_0^{lean} are the oxygen molar concentrations at the oxygen-rich and oxygen-lean surface, respectively. C_o is estimated by $C_o = (3-\delta)/V_m$, where Vm is the molar volume estimated by XRD patterns and δ is the oxygen under-stoichiometry evaluated by thermogravimetric analysis under air.

The coefficient of oxygen diffusion, expressed in cm^2s^{-1}, is calculated with the following equation:

$$D_0 = \frac{4LJ_{O_2}}{C_0\Delta\mu_{O_2}^{Bulk}} \qquad \textbf{(Eq. 7)}$$

2.5.4. Identification of the limiting step of the oxygen transport through the membrane

Oxygen transport through the membrane is governed by bulk diffusion or/and kinetics of surface exchanges. In recent works, Valentin et al [23, 24] have introduced a new criterion called B_c, which is the ratio between the chemical potential gradient at the membrane surface and the one associated to the bulk diffusion. This criterion allows to identify the limiting step of oxygen transport through the membrane.

$$B_c = \frac{\Delta\mu_{O_{2(s)}}^{lean}}{\Delta\mu_{O_2}^{Bulk}} \textbf{(Eq. 8)}$$

If B_c is lower than 0.5, the oxygen flux is mainly governed by the oxygen diffusion through the membrane, and if B_c is higher than 1.5, the oxygen flux is mainly governed by oxygen surface exchanges between the gas and the membrane surfaces. Finally, in case of B_c is between 0.5 and 1.5, this corresponds to a mixed regime where the oxygen flux is partially governed by oxygen diffusion and surface exchanges.

3. Results and discussion

3.1. The dependence of the surface quality on the oxygen semi-permeation

Figure 2 shows, a) the oxygen semi-permeation flux as function of the temperature for LSFG5573 membranes and, b) the Arrhenius plots of oxygen semi-permeation for LSFG5573 membranes with different surface roughness.

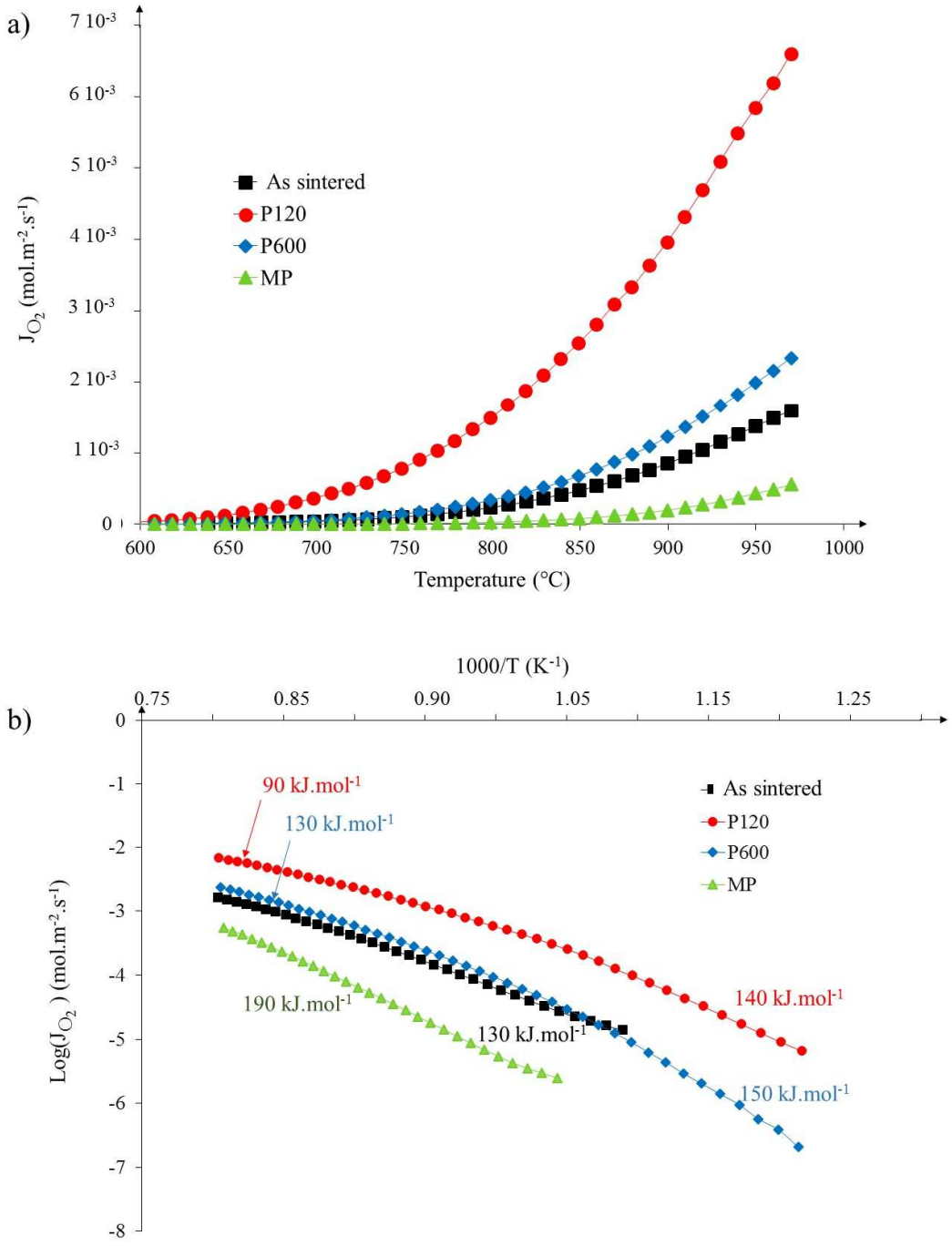

Figure 2. The oxygen semi-permeation fluxes through $LSFG_{5573}$ membranes a) function of the temperature and b) function of the surface roughness at 900 °C

Figure 2a shows a large variation of oxygen flux in relation with the surface roughness of $LSFG_{5573}$ membrane. This suggests that the oxygen flux through the $LSFG_{5573}$ membranes is mainly governed by the surface exchanges. The best oxygen semi-permeation flux is 3.9 10^{-3} mol.m^{-2}.s^{-1} at 900°C, and it is obtained with "P120"

membrane. This value of oxygen flux is close to the best performances reported in the literature with a dense membrane thickness of 1 mm. For instance, the best oxygen semi-permeation fluxes reported in the literature with $Ba_{1-x}Sr_xFe_{1-y}Co_yO_{3-\delta}$ perovskite membranes are from 1 to 20 10^{-3} $mol.m^{-2}.s^{-1}$ at 900 °C [25, 26].

Figure 3 shows the variation of Bc^{lean} criterion in relation with the temperature and the surface roughness of the membrane. Bc^{lean} is higher to 1.5 for "As sintered" and "MP" membranes, corresponding to an oxygen flux governed by surface exchanges at the oxygen lean side of the membrane, as expected. In case of P600 and P120 membranes, the variation of Bc^{lean} with the temperature shows that the oxygen flux is partially governed by oxygen diffusion at high temperature (> 900 °C), with a Bc^{lean} close to 1. In opposite case, the oxygen flux is mainly governed by surface exchange at lower temperature (< 800 °C), with a Bc^{lean} > 1.5. In consequence, the Arrhenius plots of the oxygen semi-permeation flux through the "P600" and "P120" membranes show a variation of activation energy (figure 2b), which is likely linked to a change of the limiting step of oxygen transport through the membrane with the temperature, as reported by the evolution of Bc^{lean} in figure 3.

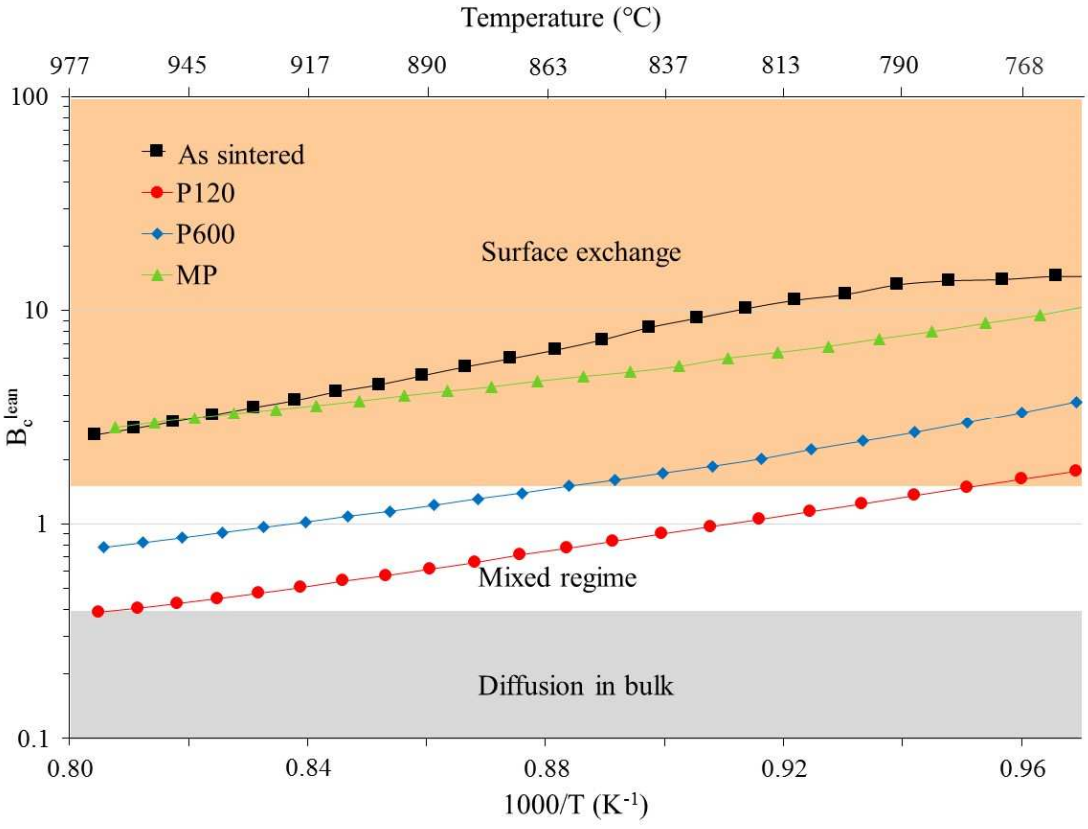

Figure 3. Variation of Bc^{lean} with temperature for different surface roughness of membranes

Besides, the activation energy is decreasing with the surface roughness of the $LSFG_{5573}$ membrane, from 130 $kJ.mol^{-1}$ for "As sintered" membrane to 190$kJ.mol^{-1}$ for "PM" membrane at high temperature. This suggests that there is an evolution of the surface exchange mechanism as function of the surface state of the membrane. This leads to understand the influence of the surface physico-chemistry on the kinetics of oxygen surface exchanges, as reported in the next section.

3.2 Understanding of the surface physico-chemistry on the kinetics of oxygen surface exchanges

The roughness of the membrane surfaces (R_a) is evaluated by interferometric microscopy. It is possible to design 3D and 2D cartographies of the surface topographies (Fig. 4). The software (Mountains Software) allows to calculate the real surface developed by the roughness from topographic data of the membrane surface. The surface developed by the roughness is determined here from the surface ratio (S_d/S_{app}) between the surface developed by the roughness (Sd) and the apparent surface of the membrane (Sapp) (Table 1). The variation of this ratios (S_d/S_{app}) remains low for the four surfaces characterized, i.e. between 1.1 and 1.4. This means that the real surface developed by the roughness is still close to the apparent surface of the membrane in this study. Tereoka et al. reported significantly higher ratios in relation with the roughness of the membrane surface, i.e. between 1.44 and 3.19 [6].

Table 1 gives the average surface roughness in relation with the abrasive paper grade used for the polishing of the membrane surface. Logically, a surface polished with a P120 paper has higher roughness (Ra= 0.86 µm) than one polished with a P600 paper (Ra= 0.54 µm). The average roughness of the mirror-polished surface membrane is very low (Ra= 0.15 µm) in comparison with other surfaces. The roughness of the membrane surface increases as following: MP < P600 < As sintered < P120.

Table 1. Roughness at the membrane surfaces obtained by interferometric microscopy

Polishing	**P120**	**As sintered**	**P600**	**MP**
Ra (µm)	0.86	0.54	0.38	0.15
S_d/S_{app}	1.4	1.2	1.1	1.1

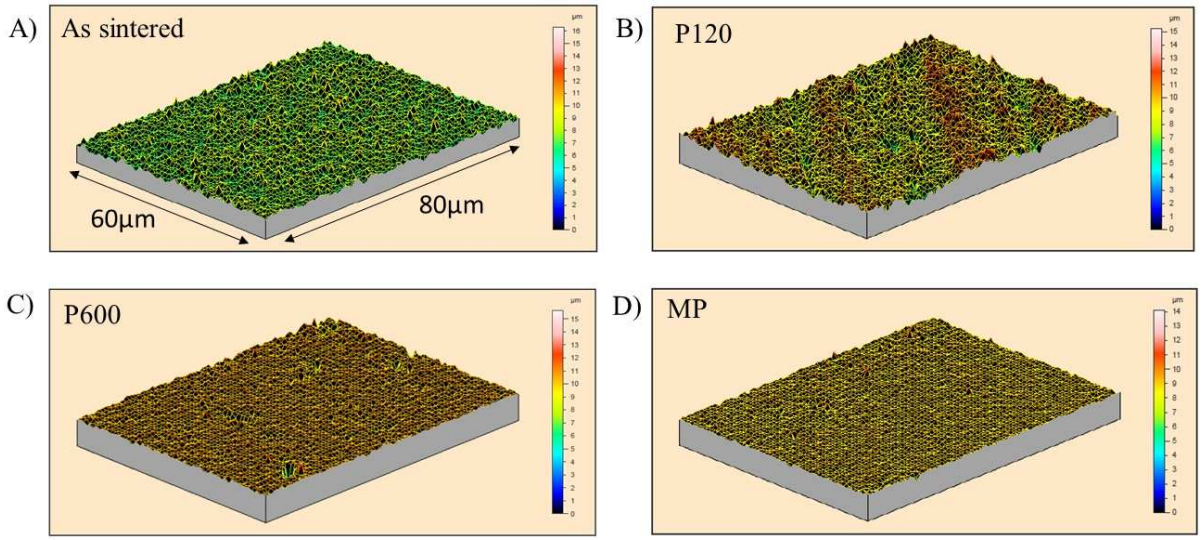

Figure 4. Cartographies of the membrane surfaces obtained by white light interferometry, A) As sintered surface, B) P120, C) P600 and D) MP.

Figure 5 shows the XRD patterns (obtained at grazing angle of 5°) recorded from the membranes with the different polishing grades. Secondary phases, such as $SrLaGa_3O_7$, are very difficult to totally eliminate by synthesis of $LSFG_{5573}$ by solid state reaction [15, 27] and this phase is observed in the as-sintered and for the first polishing state. An important outcome of these experiments is that they evidence a segregation of the $SrLaGa_3O_7$ secondary phase at the surface of $LSFG_{5573}$ membrane during the sintering. Indeed, after intense polishing of the membrane surface, the $SrLaGa_3O_7$ secondary phase is no more detected on XRD patterns, because the concentration of the $SrLaGa_3O_7$ secondary phase in bulk is too low to be detected on XRD patterns. This secondary phase is only detected at the vicinity of the surface by XRD analysis at grazing angle after sintering. Then, the surface polishing of the membrane leads to remove (totally or partially) this secondary phase at the membrane surface. From the relative intensities of the 110 peak of $LSFG_{5573}$ ($2\theta = 32.46°$) and 211 peak of $SrLaGa_3O_7$ ($2\theta = 29.91°$), and using the integrated intensity equation [28], it is possible to derive the volumic ratio of those phase. The results are shown in Table 2.

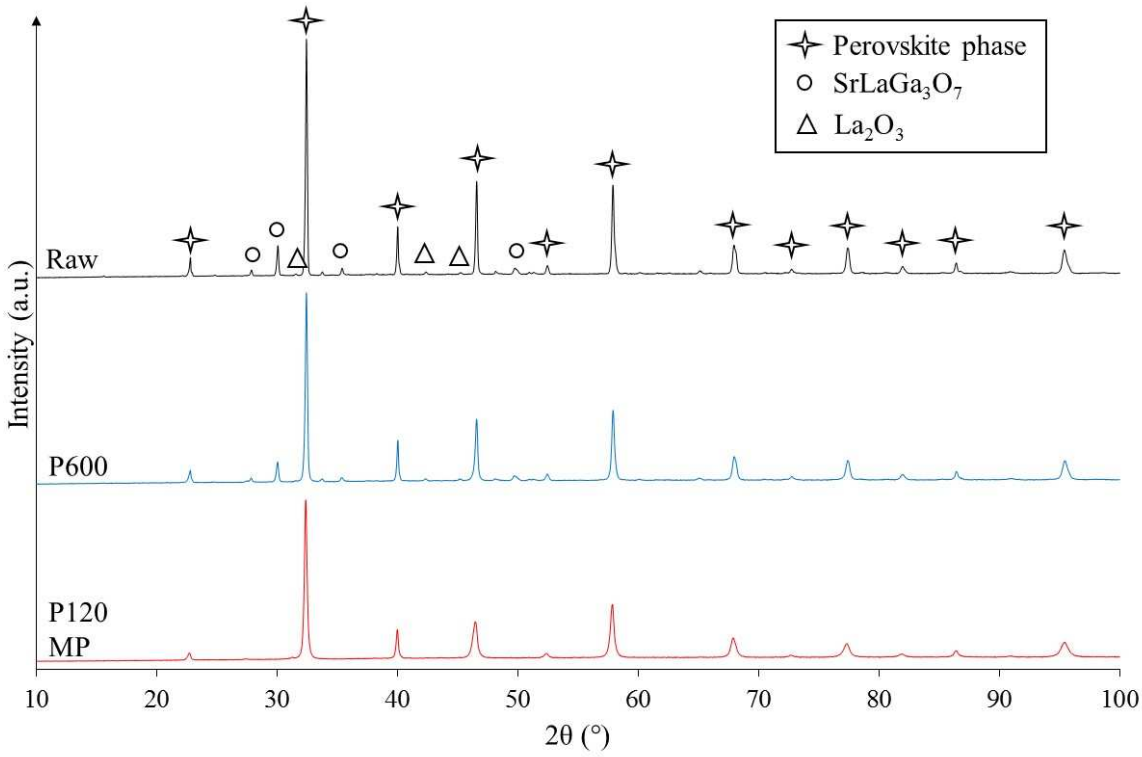

Figure 5. XRD patterns at grazing angle of $LSFG_{5573}$ membranes as function of the surface roughness

Table 2. Qualitative estimation of $SrLaGa_3O_7$ type secondary phase as function of the surface roughness

	P120	**As sintered**	**P600**	**MP**
Volumic ratio of secondary phase	No detected	~0.11	*~0.09 (lower quantity)	No detected

Figure 6 shows the effect of the roughness/secondary phase on the oxygen semi-permeation fluxes through the $LSFG_{5573}$ membranes at 900 °C. The oxygen semi-permeation fluxes obtained for "as sintered" membrane and "P600" membrane are of the same order of magnitude, i.e. 8.5 and 12 10^{-4} $mol.m^{-2}.s^{-1}$ respectively at 900 °C. It is slightly lower, i.e. 2.2 10^{-4} $mol.m^{-2}.s^{-1}$, for the membrane with a mirror-polished surface. The larger flux is obtained for the "P120" membrane with 3.9 10^{-3} $mol.m^{-2}.s^{-1}$ at 900 °C. The variation of the oxygen semi-permeation flux with the modification of the surface characteristics suggests that the oxygen surface exchange at the membrane surface is the limiting step of oxygen transport through the membrane, as discussed in the previous section.

Two contributions of the surface on the kinetics of oxygen surface exchanges can been considered to explain the evolution of oxygen flux: i) the roughness and ii) the quantity of secondary has a large effect. Considering the

first possible contribution, the variation of the membrane surface with the roughness is very low (< 1.4) in comparison with the variation of oxygen flux (an order of magnitude higher). This suggests that the variation of the exchange surface due to the roughness, in the range tested, has a low effect on the kinetics of oxygen surface exchange.

Then, the variation of oxygen flux with the different surfaces may likely be attributed mainly to the segregation of $SrLaGa_3O_7$ secondary phase during sintering. $SrLaGa_3O_7$ is reported as a dielectric material in the literature [28-30], which leads to decrease the mobility of electrons or oxygen anions at the surface of mixed electronic and ionic conductors.

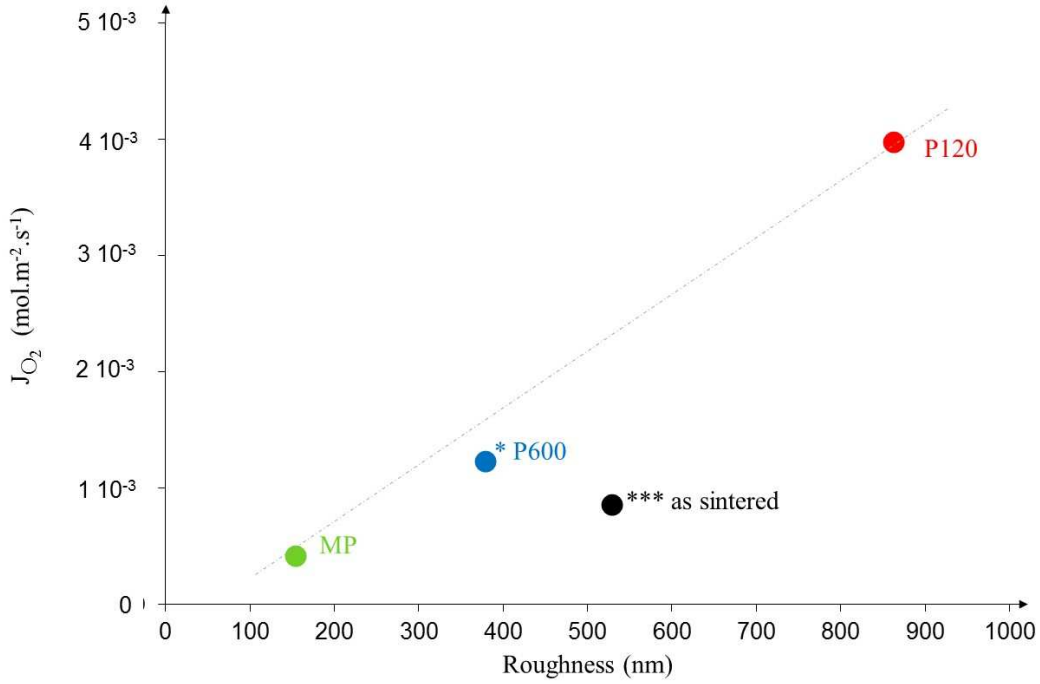

Figure 6. Effect of surface roughness on the oxygen flux through the membrane at 900 °C

Figure 7 shows the coefficients of oxygen surface exchanges at 900 °C at the oxygen rich and lean sides, in relation with the roughness (Ra). k_i and k_{des} coefficients can be attributed to the surface exchange coefficients of oxygen incorporation and oxygen desorption on each side of the membrane, because the surface of $LSFG_{5573}$ membrane is far from the equilibrium state in oxygen semi-permeation conditions. In this respect, the surface reaction can be associated to incorporation or desorption on oxygen rich and lean sides, as reported in reaction 1 and 2:

$$O_{2\,(g)} + V_O^{\bullet\bullet} \xrightarrow{k_i} O_O^X + 2\,h^{\bullet}$$ reaction 1: oxygen incorporation at the oxygen rich side

$O_O^X + 2\,h^{\bullet} \xrightarrow{k_{des}} O_{2\,(g)} + V_O^{\bullet\bullet}$ reaction 2: oxygen desorption at the oxygen lean side

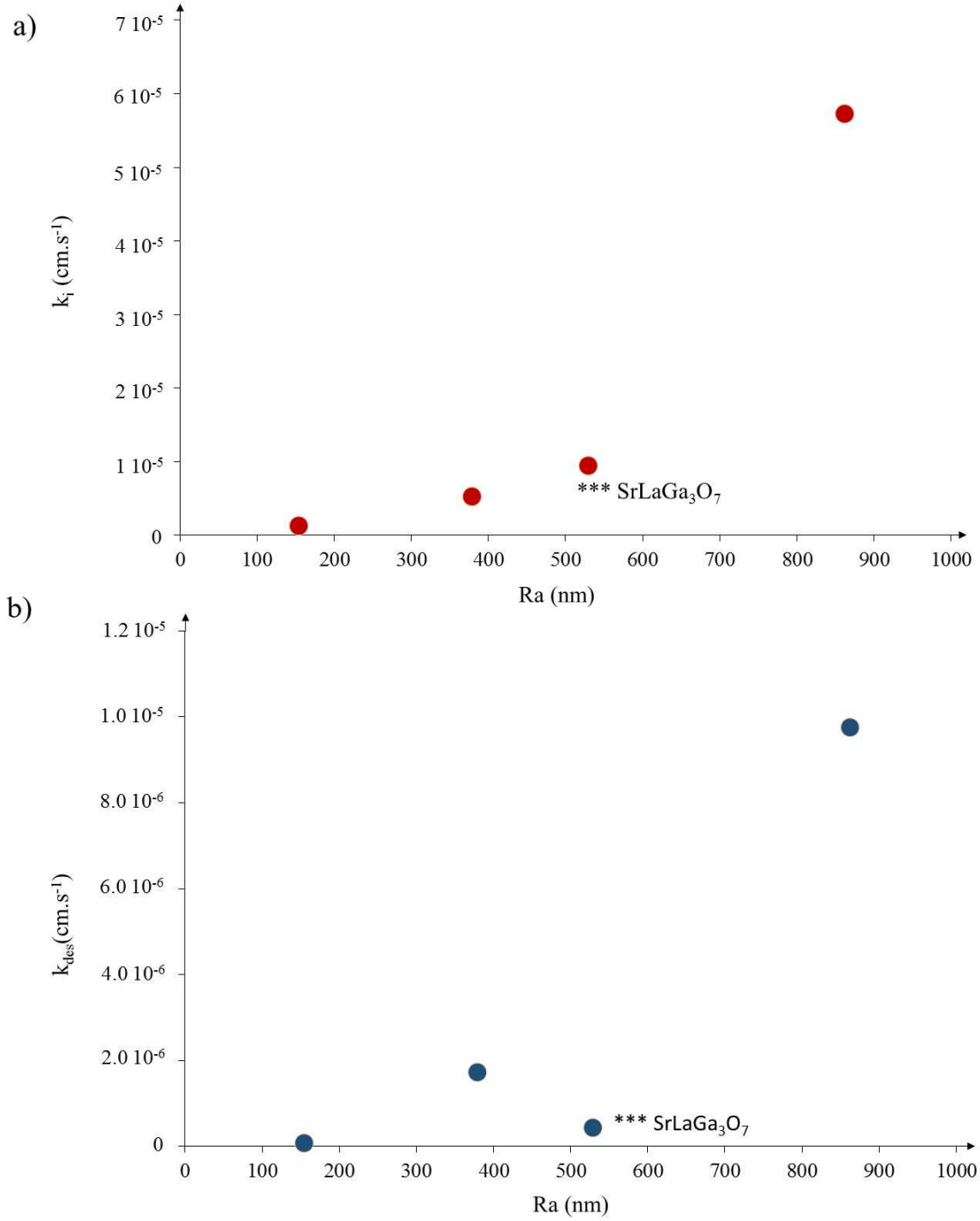

Figure 7. Effect of the roughness on the coefficients, a) of oxygen incorporation at the oxygen-rich side (k_i) and b) of oxygen desorption at the oxygen lean side (k_{des}) at 900 °C.

The coefficient of oxygen incorporation at the oxygen-rich side (k_i) of the membrane exponentially increases with the roughness of the membrane surface. There is not apparent effect of the $SrLaGa_3O_7$ secondary phase on the kinetics of incorporation of oxygen.

However, the oxygen flux through the $LSFG_{5573}$ membranes is predominantly governed by oxygen surface exchanges at the oxygen-lean side of the membrane attested by a k_i coefficient significantly larger than k_{des} coefficient for the same roughness values (Ra), 1.6 10^{-6} and 3.6 10^{-7} $cm.s^{-1}$ respectively, for P600 membrane at 900 °C (Fig.7).

The presence of $SrLaGa_3O_7$ secondary phase on the membrane surface (only for the sample noted "as sintered") seems to have a large effect on the coefficients of oxygen desorption at the oxygen lean side of the membrane. The k_{des} coefficient of the "as sintered" membrane is lower than the k_{des} coefficient of the "P600" membrane, 4.1 10^{-7} and 1.7 10^{-6} $cm.s^{-1}$ respectively, although, the roughness (Ra) of the "as sintered" membrane surface is higher than the one of the "P600" membrane surface. Besides, the $SrLaGa_3O_7$ secondary phase is a dielectric material [28-30], which leads to decrease the mobility of electrons or oxygen species at the surface of mixed conductors, and then the kinetics of oxygen desorption at the membrane surface.

Finally, the large effect of the surface roughness on the kinetic of oxygen desorption or incorporation is not well understood here. For instance, XPS analysis at the membrane surface shows not significant impurities or chemical segregations for the different surfaces reported in this work. The main assumption is that a large roughness could be favorable to increase the concentration of oxygen vacancies at the membrane surface. The oxygen vacancy concentration could be locally modified by the local surface radius at the interface solid/gas, as reported by Laplace equation in the literature on the sintering mechanism [32]. This local variation of oxygen vacancy concentration at the material surface could strongly increases the kinetics of oxygen surface or the apparent coefficients of oxygen exchanges at the membrane surfaces.

Conclusions

The surface roughness of $LSFG_{5573}$ perovskite membrane has a large effect on their oxygen semi-permeation performances. The oxygen flux through $LSFG_{5573}$ perovskite membrane is mainly governed by the kinetics of oxygen desorption at the oxygen lean side of the membrane.

Besides, the presence of $SrLaGa_3O_7$ secondary phase at the $LSFG_{5573}$ perovskite membrane largely decreases the coefficient of oxygen desorption at the oxygen lean sides. This $SrLaGa_3O_7$ secondary phase segregates at the membrane surface during sintering, and the surface polishing of the membrane leads to remove (totally or partially) this secondary phase at the membrane surface.

Then, a large roughness at the membrane surface without secondary phase leads to an increase of the kinetics of oxygen surface exchanges, and indirectly the oxygen flux through the membrane. By this way, the best oxygen fluxes obtained in this work, is 3.9 10^{-3} $mol.m^{-2}.s^{-1}$, and is not far from the best performances reported in the literature with a dense 1 mm in thick membrane.

These results require to define correctly the roughness and the physico-chemistry of the membrane surface, to evaluate the oxygen semi-permeation of the membrane materials. Finally, this work shows that it is possible to largely improve the electrochemical properties of membranes by a control of the surface physico chemistry. This could lead to a promising route for the development of new design for cathode materials for solid oxide fuel cell or for membranes for oxygen separation applications.

Acknowledgements

The authors wish to express their gratitude to Air Liquide Company for financial and technical support and the ADEME (French Environment and Energy Management Agency) for financial support of this study.

References

[1] J. Sunsaro, S. Baumann, J.M. Serra, W.A. Meulenberg, S. Liu, Y.S. Lin, J.C. Diniz da Costa, Mixed ionic-electronic conducting (MIEC) ceramic-based membranes for oxygen separation, Journal of Membrane Science, 320 (2008), 13-41.

[2] P.-M. Geffroy, J. Fouletier, N. Richet, T. Chartier, Rational selection of membrane materials of MIEC materials in energy production processes, Chemical Engineering Science, 87 (2013), 408-433.

[3] Y. Hayamizu, M. Kato, H. Takamura, Effects of surface modification on the oxygen permeation of $Ba_{0.5}Sr_{0.5}Co_{0.8}Fe_{0.2}O_{3-\delta}$, J. Membr. Sci., 462 (2014), 147-152.

[4] L. Guironnet, P.-M. Geffroy, N. Richet, T. Chartier, Improvement of oxygen flux through perovskite membranes using a coating of ultra-divided particles, Chemical Engineering science, 156 (2016), 128-135.

[5] L. Guironnet, P.-M. Geffroy, F. Jouay, C. Pagnoux, N. Richet, T. Chartier, $La_{0.6}Sr_{0.4}Fe_{0.8}Co_{0.2}O_{3-\delta}$ electrophoretic coating for oxygen transport membranes, Chemical Engineering Science: X, 2019.

[6] H. Kusaba, Y. Shibata, K. Sasaki, Y. Teraoka, Surface effect on oxygen permeation through dense membrane of mixed-conductive LSCF perovskite-type oxide, Solid State Ionics 177 (2006) 2249–2253.

[7] Jonas Gurauskis, Ørjan F.Lohne, Kjell Wiik, $La_{0.2}Sr_{0.8}Fe_{0.8}Ta_{0.2}O_{3-\delta}$ based thin film membranes with surface modification for oxygen production, Solid State Ionics, 225 (2012) 703-706.

[8] Steffen Ziesche, Robert Jurk, N. Trofimenko, M. Kusnezoff, Permeation and oxygen exchange of $Ln_2Ni_{0.8}Cu_{0.2}O_4$-materials (Ln = La, Pr, Nd), Solid State Ionics, 179, 27–32 (2008) 1351-1353.

[9] Jung Hoon Park, Jong Pyo Kim, Sou Hwan Son, Oxygen Permeation and Stability of $Ba_{0.5}Sr_{0.5}Co_{0.8}Fe_{0.2}O_{3-\delta}$ Membrane According to Trace Elements and Oxygen Partial Pressure in Synthetic Air, Energy Procedia, 1 (2009) 369-374.

[10] H.J.M. Bouwmeester, H. Kruidhof, A.J. Burggraaf, Importance of the surface kinetics as rate limiting step in oxygen permeation through mixed-conducting oxides, Solid State Ionics, 72 (1994) 185-194.

[11] Yanying Wei, Qing Liao, Zhong Li, Haihui Wang, Enhancement of oxygen permeation through U-shaped K2NiF4-type oxide hollow fiber membranes by surface modifications, Separation and Purification Technology, 110 (2013), 74-80.

[12] Han Ning, Zhang Shuguang, Meng Xiuxia, Yang Naitao, Meng Bo, Tan Xiaoyao, Liu Shaomin. Effect of enhanced oxygen reduction activity on oxygen permeation of La0.6Sr0.4Co0.2Fe0.8O3-δ membrane decorated by K2NiF4-type oxide, Journal of Alloys and Compounds, 654 (2016), 280-289.

[13] R.J. Chater, S. Carter, J.A. Kilner, B.C.H. Steele, Development of a novel SIMS technique for oxygen self-diffusion and surface exchange coefficient measurements in oxides of high diffusivity, Solid State Ionics, 53-56 (1992) 859-867.

[14] A. Vivet, P.-M. Geffroy, P. Del Gallo, T. Chartier, N. Richet, $La_{(1-x)}Sr_xFe_{(1-y)}Ga_yO_{3-\delta}$ perovskite membrane, oxygen semi-permeation, thermal expansion coefficient and chemical stability under reducing conditions, J. Membrane Science, 372 (1-2) (2011), 373-379.

[15] P.-M. Geffroy, M. Reichmann, L.Kilmann, J. Jouin, N. Richet, T. Chartier, Identification of the rate-determining step in oxygen transport through $La_{(1-x)}Sr_xFe_{(1-y)}Ga_yO_{3-\delta}$ perovskite membranes, Journal of Membrane Science, 476 (2015), 340-347.

[16] T. Chartier, Tape casting, The Encyclopedia of Advanced Materials, vol. 4, Pergamon, Cambridge (1994) 1763-1767.

[17] A. Vivet, P.-M. Geffroy, E. Thune, C. Bonhomme, F. Rossignol, N. Richet et T. Chartier, New route for high oxygen semi-permeation through surface-modified dense $La_{1-x}Sr_xFe_{1-y}GayO_{3-\delta}$ pérovskite membranes, Journal of Membrane Science, 454, (2014), 97-108.

[18] P.-M. Geffroy, A. Vivet, J. Fouletier, C. Steil, E. Blond, N. Richet, P. Del Gallo, T. Chartier, The effect of experimental factors on oxygen semi-permeation measurements, Journal of Electrochemical Society, 160 (1) (2013), 1-9.

[19] A. Vivet, P.-M. Geffroy, V. Coudert, J. Fouletier, T. Chartier, N. Richet, Influence of glass and gold sealants materials on oxygen permeation performances in $La_{0.8}Sr_{0.2}Fe_{0.7}Ga_{0.3}O_{3-\delta}$ perovskite membranes, Journal of Membrane Science, 366 (1-2) (2011), 132-138.

[20] J. Fouletier, P. Fabry, M. Kleitz, Electrochemical semipermeability and the Electrode Microsystem in Solid Oxide Electrolyte Cell, Journal of the electrochemical society, 1976, 123 (2), 203-2013.

[21] M.Z. Bazant, Theory of chemical kinetics and charge transfer based on nonequilibrium thermodynamics, Accounts of chemical research 46, 5 (2013), 1144-1160.

[22] S.B. Adler, X.Y. Chen, J.R. Wilson, Mechanisms and rate laws for oxygen exchange on mixed-conducting oxide surfaces, Journal of Catalysis, 245 (2007), 91-109.

[23] O. Valentin, E. Blond, N. Richet, Themo-chemico-mechanical modelling of mixed conductors in transient stages, Advances in Science and Technology, 65 (2010), 232–237.

[24] P.-M. Geffroy, E. Blond, N. Richet, T. Chartier, Understanding and identifying the oxygen transport mechanisms through mixed-conductor membranes, Chemical Engineering Sciences, 162 (2017) 245-261.

[25] L. Ge, R. Ran, K. Zhang, S. Liu, Z. Shao, Oxygen selective membranes based on B-site cation-deficient $(Ba_{0.5}Sr_{0.5})(Co_{0.8}Fe_{0.2})yO_{3-\delta}$ perovskite with improved operational stability, J. Membr. Sci. 318 (2008) 182.

[26] L. Ge, Z. Shao, K. Zhang, R. Ran, J.C. Diniz da Costa, S. Liu, Evaluation of Mixed-Conducting Lanthanum-Strontium-Cobaltite Ceramic Membrane for Oxygen Separation, AIChE Journal 55 (2009) 2603.

[27] V.V. Kharton, A.L. Shaulo, A.P. Viskup, M. Avdeev, A.A. Yaremchenko, M.V. Patrakeev, A.I. Kurbakov, E.N. Naumovich and F.M.B. Marques, Perovskite-like system (Sr,La)(Fe,Ga)$O_{3-\delta}$: Structure and ionic transport under oxidizing conditions, Solid State Ionics, 150 (2002), 229-43.

[28] B. E. Warren, X-ray diffraction, New-York: Addison Wesley, 1969

[26] J. Konopka, I. Wolff, IEEE Transactions on Microwave Theory and Techniques, 40 (1992) 2418-2423.

[29] J. Xu, X. Li, F. Lu, H. Fu, C. Brown, X. Kuang, Oxygen interstitials and vacancies in $LaSrGa_3O_7$-based melilites, Journal of Solid State Chemistry, 230 (2015), 309-217.

[30] K. Huang, R.S. Tichy, J.B. Goodenough, Superior perovskite oxide-ion conductor; strontium- and magnesium-doped $LaGaO_3$, Journal of the American Ceramic Society, 81(10) (1998), 2576-2580.

[31] Didier Bernache-Assollant, Chimie-Physique du frittage, Hernès Science Publications, Forceram, 1993.

Table captions

Table 1. Roughness at the membrane surfaces obtained by interferometric microscopy

Table 2. Qualitative estimation of $SrLaGa_3O_7$ type secondary phase as function of the surface roughness

Figure captions

Figure 1. Oxygen semi-permeation setup and its microelectrodes system

Figure 2. The oxygen semi-permeation fluxes through $LSFG_{5573}$ membranes a) function of the temperature and b) function of the surface roughness at 900 °C

Figure 3. Variation of Bc^{lean} with temperature for different surface roughness of membranes

Figure 4. Cartographies of the membrane surfaces obtained by white light interferometry, A) As sintered surface, B) P120, C) P600 and D) MP.

Figure 5. XRD patterns at grazing angle of $LSFG_{5573}$ membranes as function of the surface roughness

Figure 6. Effect of surface roughness on the oxygen flux through the membrane at 900 °C

Figure 7. Effect of the roughness on the coefficients, a) of oxygen incorporation at the oxygen-rich side (k_i) and b) of oxygen desorption at the oxygen lean side (k_{des}) at 900 °C.